Earth's Future

RESEARCH ARTICLE
10.1029/2025EF007346

Tropical Salinity Contrast Strengthening in CMIP6: Inter-Model Diversity and Mechanisms

Shanshan Pang[1,2,3], **Jérôme Vialard**[4], **Matthieu Lengaigne**[1], **and Xidong Wang**[2,3]

[1]MARBEC, Université de Montpellier, CNRS, Ifremer, IRD, Sète, France, [2]Key Laboratory of Marine Hazards Forecasting, Ministry of Natural Resources, Hohai University, Nanjing, China, [3]College of Oceanography, Hohai University, Nanjing, China, [4]LOCEAN-IPSL, IRD-CNRS-MNHN-Sorbonne Université, Paris, France

Key Points:

- Two inter-basin indices explain 76% of CMIP6 diversity in tropical SSS projections and capture opposing inter-basin responses
- Indo-Pacific salinity changes mirror rainfall shifts driven by warming patterns through "warmer gets wetter" mechanisms
- Atlantic salinity changes are driven by increased evaporation under warming through "dry gets drier" mechanisms

Supporting Information:

Supporting Information may be found in the online version of this article.

Correspondence to:

S. Pang,
shanshan.pang@ird.fr

Citation:

Pang, S., Vialard, J., Lengaigne, M., & Wang, X. (2026). Tropical salinity contrast strengthening in CMIP6: Inter-model diversity and mechanisms. *Earth's Future*, *14*, e2025EF007346. https://doi.org/10.1029/2025EF007346

Received 21 MAY 2024
Accepted 19 DEC 2025

Author Contributions:

Conceptualization: Shanshan Pang, Jérôme Vialard, Matthieu Lengaigne
Data curation: Shanshan Pang
Formal analysis: Shanshan Pang, Jérôme Vialard, Matthieu Lengaigne
Investigation: Shanshan Pang, Jérôme Vialard, Matthieu Lengaigne
Methodology: Shanshan Pang, Jérôme Vialard, Matthieu Lengaigne
Resources: Shanshan Pang
Software: Shanshan Pang
Supervision: Jérôme Vialard, Matthieu Lengaigne, Xidong Wang
Visualization: Shanshan Pang
Writing – original draft: Shanshan Pang
Writing – review & editing: Jérôme Vialard, Matthieu Lengaigne

Abstract We analyze projected tropical sea surface salinity (SSS) changes in 32 CMIP6 models' historical and SSP5-8.5 scenario simulations, examining both the multi-model mean (MMM) and inter-model diversity. By 2100, MMM inter-basin contrasts strengthen, with freshening in the tropical Indian Ocean (TIO) and equatorial-northern Pacific (ENPO), and saltening in the southern Pacific (SPO) and tropical Atlantic (TAO). Basin-scale future SSS changes are primarily driven by surface freshwater fluxes, with lateral advection redistributing anomalies within each basin. Precipitation dominates the freshwater flux changes, except in the tropical Atlantic where evaporation plays a key role. Two uncorrelated indices, contrasting SPO versus TIO and TAO versus ENPO, explain 76% of the variance across models. Physically, stronger relative warming of the Northern Hemisphere enhances rainfall over the TIO monsoon region (freshening) while suppressing rainfall along the South Pacific Convergence Zone (saltening). The increasing TAO–ENPO contrast arises from two distinct mechanisms: in the Pacific, an enhanced El Niño–like warming pattern reduces atmospheric stability, intensifying rainfall and freshening ENPO; in the Atlantic, saltening reflects stronger evaporation under warmer conditions, though at a weaker rate than predicted by Clausius–Clapeyron scaling (~4.2 vs. ~7% K^{-1}). Previous studies linked strengthening of inter-basin salinity gradients to a thermodynamically intensified hydrological cycle. Our analysis highlights a more nuanced picture: Atlantic saltening reflects this thermodynamic control, while SSS changes elsewhere are mainly driven by atmospheric circulation and rainfall changes tied to uneven SST warming. The CMIP6 statistical analyses highlight dynamical mechanisms that motivate further testing through targeted ocean simulations.

Plain Language Summary Observations and climate models show that sea surface salinity (SSS) contrasts between tropical ocean basins are increasing under climate change. This pattern is often interpreted as a fingerprint of an intensifying hydrological cycle: wet regions getting wetter, dry regions getting drier. We test this idea using projections from 32 climate models. At the scale of entire ocean basins, SSS changes generally track rainfall, except in the Atlantic where evaporation dominates. Yet the story is more complex than a simple intensification of the hydrological cycle. Where the oceans warm the most also matters: stronger warming reduces atmospheric stability, making it easier for air to rise and produce rainfall. As a result, Indo-Pacific regions that warm most tend to freshen, while regions that warm least tend to become saltier. The Atlantic, by contrast, becomes saltier mainly because warming enhances evaporation, consistent with the "wet-gets-wetter, dry-gets-drier" view. Overall, our results confirm that basin-scale salinity changes act as "nature's rain gauge," recording long-term shifts in rainfall and evaporation. They also reveal that different mechanisms drive salinity changes across basins: hydrological cycle intensification in some regions, and rainfall shifts linked to uneven ocean warming in others.

1. Introduction

Anthropogenic radiative forcing, mainly from rising atmospheric greenhouse gas concentrations, has caused a global mean surface warming of more than 1.2 K by 2020 relative to pre-industrial levels (IPCC, 2021). Over 90% of the associated excess heat has been absorbed by the oceans, driving ocean warming, sea level rise, and sea ice loss (IPCC, 2021). Climate change also affects ocean salinity, which matters because salinity influences seawater density and upper-ocean stratification (Capotondi et al., 2012). This can, for instance, impact the strength of the Atlantic Meridional Overturning Circulation (e.g., He & Clark, 2022; Manabe & Stouffer, 1995; Rahmstorf, 1995) and induce a weak negative feedback on global warming (Williams et al., 2007). In addition, long-term changes in sea surface salinity (SSS) provide a valuable fingerprint of shifts in rainfall under climate change:

salinity effectively acts as "nature's rain gauge" (Cravatte et al., 2009; Curry et al., 2003; Durack et al., 2012; Durack & Wijffels, 2010; Helm et al., 2010; Hosoda et al., 2009; Schmitt, 2008; Skliris et al., 2014; Terray et al., 2012; Yu, 2011).

Many studies of salinity changes under global warming have focused on high latitudes, particularly the Arctic (e.g., Khosravi et al., 2022; Shu et al., 2018), where salinity exerts a strong control on stratification (Capotondi et al., 2012). Yet salinity is also important in the tropics, where it can influence the development of high-impact climate phenomena such as El Niño (e.g., Vialard & Delecluse, 1998; Wang et al., 2024) and tropical cyclones (e.g., Balaguru et al., 2020). Rainfall shifts in the tropics under climate change could affect billions of people, and SSS provides a powerful means to monitor these changes as "nature's rain gauge" (e.g., Durack et al., 2012; Terray et al., 2012).

Only a handful of studies have examined how tropical SSS responds to anthropogenic forcing using the Coupled Model Intercomparison Project (CMIP) database, and they consistently report Indo-Pacific freshening and Atlantic saltening (Capotondi et al., 2012; Li et al., 2023; Sathyanarayanan et al., 2021; Sun & Du, 2023). This corresponds to a strengthening of inter-basin salinity gradients—a saltier Atlantic and a fresher Indo-Pacific—commonly interpreted as a fingerprint of changes in the hydrological cycle (Cravatte et al., 2009; Curry et al., 2003; Durack et al., 2012; Durack & Wijffels, 2010; Helm et al., 2010; Hosoda et al., 2009; Schmitt, 2008; Skliris et al., 2014; Terray et al., 2012; Yu, 2011). At the basin scale, those SSS trends generally track freshwater flux (evaporation minus precipitation, hereafter E–P) changes (Sathyanarayanan et al., 2021; Sun & Du, 2023), but regional patterns can be modified by lateral advection (Vinogradova & Ponte, 2013; Yu, 2011), circulation shifts (Ge et al., 2023), and internal variability (e.g., Du et al., 2015; Sun et al., 2021). In addition, upper-ocean warming increases vertical stratification, amplifying the salinity response to E–P anomalies (Zika et al., 2018).

E–P responds to two key mechanisms, often referred to as "wet gets wetter" and "warmer gets wetter" (Allan et al., 2020; Zaitchik et al., 2023). The "wet gets wetter" (and "dry gets drier") response follows from the basic thermodynamics of a warmer atmosphere (Clausius–Clapeyron), neglecting circulation changes. A warmer atmosphere increases evaporation at 7% K^{-1} in the absence of wind or relative humidity changes (Allen & Ingram, 2002; Huntington, 2006; Roderick et al., 2015), leading to saltening where evaporation dominates ("dry gets drier"). It also strengthens horizontal humidity gradients, enhancing rainfall in already wet regions and suppressing it in dry ones (Held & Soden, 2006). CMIP6 high-emission simulations (SSP5-8.5) indeed project increased evaporation over the tropical oceans (Figure 1c) and a tendency toward more rainfall in wet regions and less in dry ones (Figure 1b), commonly interpreted as hydrological cycle intensification (Allan et al., 2020; Allen & Ingram, 2002; Chou & Neelin, 2004; Held & Soden, 2006), based on 2071–2100 changes relative to the 1985–2014 climatology.

This framework, however, neglects circulation changes tied to sea surface temperature (SST) patterns—a mechanism termed "warmer gets wetter" (Chou & Neelin, 2004; Xie et al., 2010). Relative SST (RSST, SST minus its tropical mean) provides a useful proxy for atmospheric stability and its changes (Izumo et al., 2020; Xie et al., 2010). Precipitation tends to increase where RSST is positive and decrease where it is negative (Figures 1a and 1b), as seen in CMIP6 projections of enhanced equatorial Pacific warming and rainfall. On larger scales, stronger Northern Hemisphere warming shifts the Intertropical Convergence Zone (ITCZ) northward to maintain hemispheric energy balance (Bollasina et al., 2011; Chung & Ramanathan, 2006; Friedman et al., 2013; Guilbert et al., 2024; Kang, 2020; Liu & Chiang, 2012), analogous to its seasonal migration in monsoon regions. In what follows, we refer to rainfall responses to both regional RSST anomalies and the interhemispheric RSST gradient as "warmer gets wetter." In practice, "wet gets wetter" (thermodynamic intensification of evaporation and moisture gradients) and "warmer gets wetter" (circulation and moisture transport changes linked to SST patterns) operate together; although effects of circulation changes usually dominate changes in rainfall (Allan et al., 2020; Zaitchik et al., 2023).

Earlier CMIP studies focused on single models, small ensembles, or idealized abrupt-4xCO2 experiments (e.g., Capotondi et al., 2012; Li et al., 2023; Sathyanarayanan et al., 2021; Sun & Du, 2023). They did not explore more realistic scenarios or the inter-model diversity of future SSS changes. Because projected rainfall shifts—and hence E–P—vary greatly across models, understanding the sources of this diversity is key to interpreting SSS responses. Here we analyze tropical SSS changes in 32 CMIP6 models under historical and SSP5-8.5 forcing, with a focus on the processes that control inter-model diversity. Specifically, we ask: (1) Are basin-scale SSS

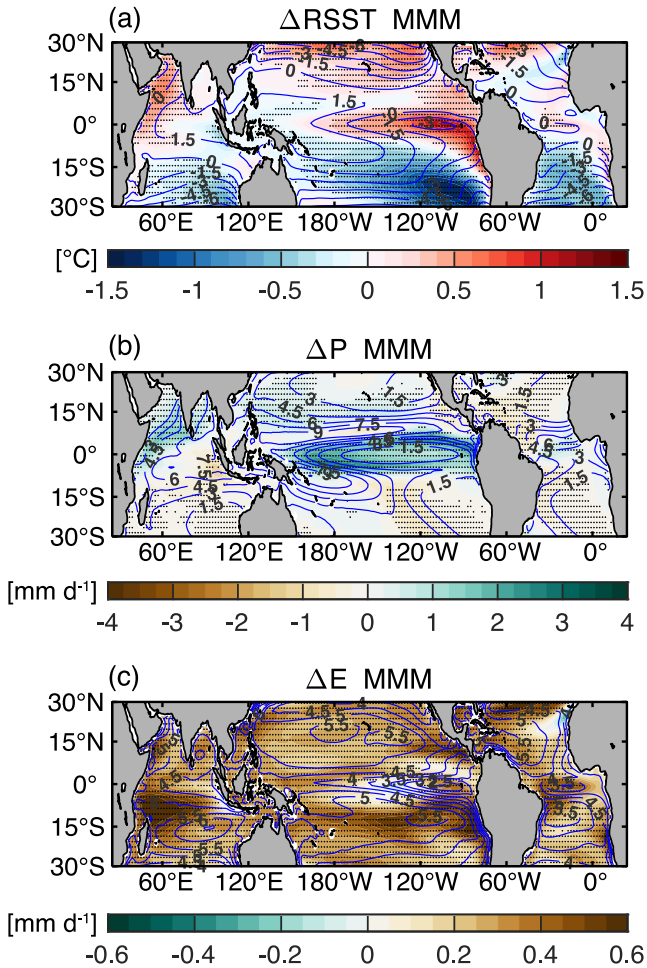

Figure 1. Projected CMIP6 changes. CMIP6 multi-model mean (MMM) annual-mean projected changes (shading) and present-day values (contours) for: (a) relative SST [RSST, defined as SST minus the tropical mean over 20°S–20°N] (°C; contour interval 1.5 °C), (b) precipitation (mm day^{-1}; contour interval 1.5 mm day^{-1}), and (c) evaporation (mm day^{-1}; contour interval 0.5 mm day^{-1}). Present-day values are defined as the 1985–2014 average of historical simulations. Projected changes are calculated as the future average under the SSP5-8.5 scenario (2071–2100) minus present-day values. Dots mark regions where 75% of the models agree with the sign of the MMM change.

changes primarily driven by E–P? (2) What are the relative roles of evaporation and precipitation? (3) Can changes in evaporation and precipitation be linked to SST (and RSST) through the "wet-gets-wetter" and "warmer-gets-wetter" mechanisms? and (4) Does the strengthening of inter-basin tropical SSS contrasts reflect an intensification of the hydrological cycle?

Section 2 describes the data and methods. Section 3 presents the multi-model mean (MMM) SSS changes and introduces four analysis regions: the tropical Indian Ocean (TIO), southern Pacific Ocean (SPO), equatorial-northern Pacific Ocean (ENPO), and tropical Atlantic Ocean (TAO) (Figure 2). We then define two uncorrelated inter-basin contrast indices—SPO–TIO and TAO–ENPO—that together account for 76% of the inter-model variance. The distinct SSS changes captured by these indices are analyzed in Section 4 (TIO vs. SPO) and Section 5 (ENPO vs. TAO). Section 6 summarizes the results and places them in the context of previous studies.

2. Data Sets and Methods

2.1. Data

We used CMIP6 historical and SSP5-8.5 scenario simulations (Eyring et al., 2016). The SSP5-8.5 scenario reflects a high-end scenario with little-to-no mitigation, fossil fuel-reliant pathway, leading to a radiative forcing of 8.5 W m^{-2} by 2100. We used the first ensemble member (r1i1p1f1) for each CMIP6 model to ensure consistency across the analysis. An assessment using all seven IPSL-CM6A-LR members—representative of the behavior seen in other models with multiple realizations—shows that the forced SSS response is highly robust across ensemble members (Text S1 and Figure S1 in Supporting Information S1), indicating that internal variability does not significantly affect the projected SSS pattern. 32 CMIP6 models listed in Table 1 were employed in the study, selected based on the availability of required variables when initiating this study. Monthly SST, SSS, precipitation rate, evaporation rate, and near-surface currents were averaged annually. In this study, surface freshwater flux is represented by E–P; river runoff from major tropical rivers (e.g., Amazon, Congo, Ganges) is not included, as its influence is mainly confined to coastal regions near the river mouths (e.g., Akhil et al., 2016; Hochet et al., 2025; Thouvenin-Masson et al., 2024). To compare the models at the same spatial scale, all data were regridded to a common resolution of 0.5°. Throughout the paper, differences between the time averages of the 2071–2100 (i.e., future climate state derived from SSP5-8.5 output) and 1985–2014 (i.e., present-day climate state derived from historical simulations) periods are referred to as projected changes (noted Δ). "MMM" refers to the multi-model mean of the 32 CMIP6 models used in this study.

2.2. Analysis Methods

Statistical significance is tested using Student's *t*-test for regressions and correlations with the degrees of freedom estimated as $N - 1$, where N is the number of models. We use pattern correlation based on Spearman's rank correlation coefficient to examine the monotonic relationship between two different maps.

To examine the inter-model spread of projected SSS change, we apply a multiple linear regression to separate and quantify the relative contributions of inter-basin SSS contrast across distinct regions. Two independent indices (justified in Section 3) are defined to represent inter-basin SSS contrasts: (a) the SPO–TIO SSS contrast index ($I_{SPO-TIO}$), defined as the normalized difference in SSS change between the SPO [145°E–70°W, 30°S–10°S] (green box on Figure 2a) and the TIO [40°E–100°E, 10°S–30°N] (orange box on Figure 2a) [that is, $\Delta SSS_{SPO} - \Delta SSS_{TIO}$]; (b) the TAO–ENPO SSS contrast index ($I_{TAO-ENPO}$), defined in the same way as $I_{SPO-TIO}$,

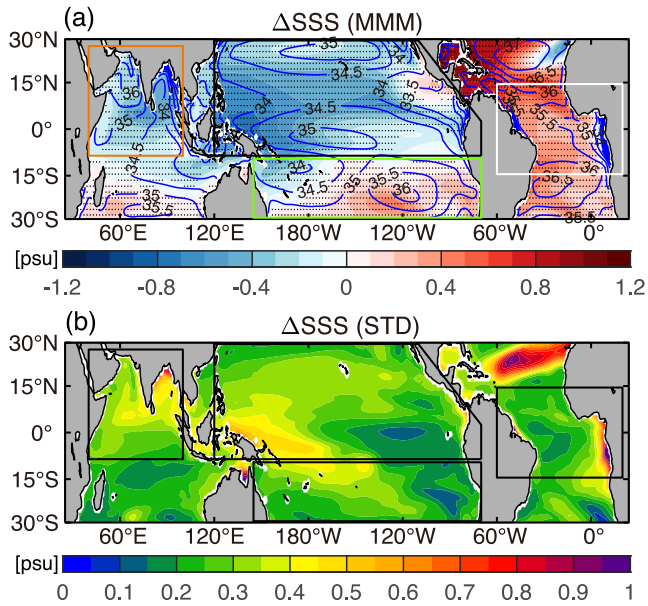

Figure 2. Projected CMIP6 SSS changes. (a) MMM annual-mean projected changes (shading) and present-day values (contours) for SSS (psu; contour interval 0.5 psu), using the same definitions as in Figure 1. Boxes in (a) denote the tropical Indian Ocean (TIO; 40°E–100°E, 10°S–30°N; orange), the southern Pacific Ocean (SPO; 145°E–70°W, 30°S–10°S; green), the equatorial-northern Pacific Ocean (ENPO; 120°E–70°W, 10°S–30°N; black) and the tropical Atlantic Ocean (TAO; 60°W–20°W, 15°S–15°N; white). (b) Inter-model standard deviation (STD) of projected SSS changes (psu) across 32 CMIP6 models (see Table 1).

but using the TAO [60°W–20°W, 15°S–15°N] (white box on Figure 2a) and the ENPO [120°E–70°W, 10°S–30°N] (black box on Figure 2a) [i.e., $\Delta SSS_{TAO} - \Delta SSS_{ENPO}$]. The bilinear regression model is formulated as.

$$\Delta SSS_{fit}(s,m) = b1(s) \times I_{SPO-TIO}(m) + b2(s) \times I_{TAO-ENPO}(m) + a + \epsilon(s,m)$$

where ΔSSS_{fit} is the fitted SSS change as a function of space (s) and model (m). The indices $I_{SPO-TIO}$ and $I_{TAO-ENPO}$ are normalized so that the regression coefficient maps $b1$ and $b2$ represent the amplitude of the inter-model diversity and can be directly compared. The constant term a represents the intercept of the regression and ϵ is the residual term.

RSST is defined as SST minus its tropical [180°W–180°E, 20°S–20°N] mean, as suggested by previous studies (e.g., Izumo et al., 2020; Van Oldenborgh et al., 2021). Two climate indices are defined in our analysis: (a) the tropical-mean warming index is calculated as the SST change averaged over tropical oceans; (b) the interhemispheric RSST gradient index is defined as the difference in RSST change between the Southern [180°W–180°E, 30°S–10°S] and Northern [180°W–180°E, 10°N–30°N] tropics (i.e., $\Delta RSST_{South} - \Delta RSST_{North}$), based on Figure 5d.

3. Tropical Projected SSS Change and Its Diversity

The CMIP6 MMM under the SSP5-8.5 scenario projects an enhanced SSS contrast with a fresher TIO and ENPO, and a saltier SPO and TAO (Figure 2a). This "fresh gets fresher" pattern is consistent with previous studies (Sathyanarayanan et al., 2021; Sun & Du, 2023). The signal is robust, with over 75% of models agreeing on the sign of change across most of the tropics (dots in Figure 2a). Despite this agreement, inter-model spread is substantial (Figure 2b): while the MMM change typically reaches 0.5 psu, the inter-model standard deviation exceeds 0.3 psu in many regions. We refer to this spread as "inter-model diversity" and analyze its structure below.

To characterize the large inter-model diversity of tropical SSS changes in CMIP6 projections, we define two indices that track inter-basin contrasts: one between the SPO and TIO, and another between the TAO and ENPO. These choices, directly guided by an Empirical Orthogonal Function analysis of inter-model diversity (Text S2 and Figure S2 in Supporting Information S1) and the statistical independence of these inter-basin contrasts (Text S2 and Table S1 in Supporting Information S1), are supported by the strong anticorrelation between paired regions, and by the fact that together they explain 76% of the inter-model variance in projected SSS changes (see below). SPO and TIO changes are anticorrelated ($r = -0.69$, $p < 0.01$), with SPO changes about half the amplitude of those in the TIO (Figure 3a). Similarly, ENPO and TAO changes are anticorrelated ($r = -0.60$, $p < 0.01$), with ENPO changes about half the size of those in the TAO (Figure 3b). The two indices are independent ($r = 0.02$, $p = 0.9$; Table S1 in Supporting Information S1) and thus capture regionally distinct aspects of SSS diversity. Present-day basin-mean contrasts in the MMM are 0.29 psu (SPO–TIO) and 1.05 psu (TAO–ENPO); projected changes strengthen these contrasts by 0.35 and 0.66 psu on average, respectively, but with wide spread across models (Table 2). All models show an increased TAO–ENPO contrast ranging from 0 to 1.64 psu, whereas SPO–TIO changes range from −0.3 to +1.3 psu, indicating large diversity in tropical SSS response.

We use a multiple linear regression model (see Section 2) to isolate the SSS patterns associated with the two indices. Together, they explain 76% of the total inter-model variance. The reconstructed SSS changes correlate above 0.7 with CMIP6 projections across most of the tropics (Figure 4a). The SPO–TIO index captures opposite SSS changes between these two basins (Figure 4b), reflecting diversity in the MMM strengthening of their SSS contrast. The TAO–ENPO index similarly represents a modulation of the MMM contrast between those two regions (Figure 4c). Because the indices are independent and regionally distinct, this two-index framework organizes the diversity into physically interpretable Indo-Pacific and Atlantic-Pacific modes: Section 4 examines

Table 1
List of CMIP6 Climate Models Considered in This Study

Label number	Model name	Modeling center, country	Horizontal resolution (lon × lat)	
			Ocean	Atmosphere
1	ACCESS-CM2	CSIRO-ARCCSS, Australia	360 × 300	192 × 144
2	ACCESS-ESM1-5	CSIRO, Australia	360 × 300	192 × 145
3	AWI-CM-1-1-MR	AWI, Germany	830,305 wet nodes	384 × 192
4	BCC–CSM2–MR	BCC, China	360 × 232	320 × 160
5	CanESM5	CCCma, Canada	360 × 291	128 × 64
6	CAS-ESM2-0	CAS, China	360 × 196	256 × 128
7	CESM2	NCAR, USA	320 × 384	288 × 192
8	CMCC-CM2-SR5	CMCC, Italy	362 × 292	288 × 192
9	CMCC-ESM2	CMCC, Italy	362 × 292	288 × 192
10	E3SM–1–0	E3SM-project, DOE, USA	30–60 km	110 km
11	E3SM–1–1	E3SM-project, DOE, USA	30–60 km	110 km
12	E3SM-1-1-ECA	E3SM-project, DOE, USA	30–60 km	110 km
13	EC–Earth3	EC-Earth consortium, Europe	362 × 292	512 × 256
14	EC-Earth3-CC	EC-Earth consortium, Europe	362 × 292	512 × 256
15	EC-Earth3-Veg	EC-Earth consortium, Europe	362 × 292	512 × 256
16	EC-Earth3-Veg-LR	EC-Earth consortium, Europe	362 × 292	320 × 160
17	FGOALS–f3–L	CAS, China	360 × 218	288 × 180
18	FGOALS–g3	CAS, China	360 × 218	180 × 80
19	GFDL–CM4	NOAA-GFDL, USA	1440 × 1080	288 × 180
20	GFDL–ESM4	NOAA-GFDL, USA	720 × 576	288 × 180
21	IITM-ESM	CCCR, India	360 × 200	192 × 94
22	INM–CM4–8	INM, Russia	360 × 318	180 × 120
23	INM–CM5–0	INM, Russia	720 × 720	180 × 120
24	IPSL–CM6A–LR	IPSL, France	362 × 332	144 × 143
25	KACE-1-0-G	NIMS-MKA, South Korea	360 × 200	192 × 144
26	MIROC6	MIROC, Japan	360 × 256	256 × 128
27	MPI–ESM–1–2–HR	MPI, Germany	802 × 404	384 × 192
28	MPI–ESM–1–2–LR	MPI, Germany	256 × 220	192 × 96
29	MRI–ESM2–0	MRI, Japan	360 × 363	320 × 160
30	NESM3	NUIST, China	362 × 292	192 × 96
31	NorESM2–LM	NCC, Norway	360 × 385	144 × 96
32	NorESM2-MM	NCC, Norway	360 × 385	288 × 192

SPO–TIO diversity linked to interhemispheric RSST gradients, while Section 5 analyzes TAO–ENPO diversity tied to the amplitude and pattern of tropical warming.

4. Tropical Indian Ocean and Southern Pacific Ocean SSS Gradient Diversity

The CMIP6 MMM projects an increasing SPO–TIO contrast, with the salty southern Pacific ocean become saltier and fresh tropical Indian Ocean becoming fresher. In this section, we examine the diversity in this projected contrast and its drivers. Associated changes in SSS, rainfall, evaporation, and RSST are identified through regression on the normalized index (Figure 5). A stronger SPO–TIO SSS contrast (Figure 5a) is linked to an enhanced interhemispheric RSST gradient, with relative cooling in the Southern Hemisphere and warming in the Northern Hemisphere (Figure 5d). Previous studies show that such gradients drive a northward shift of rainfall

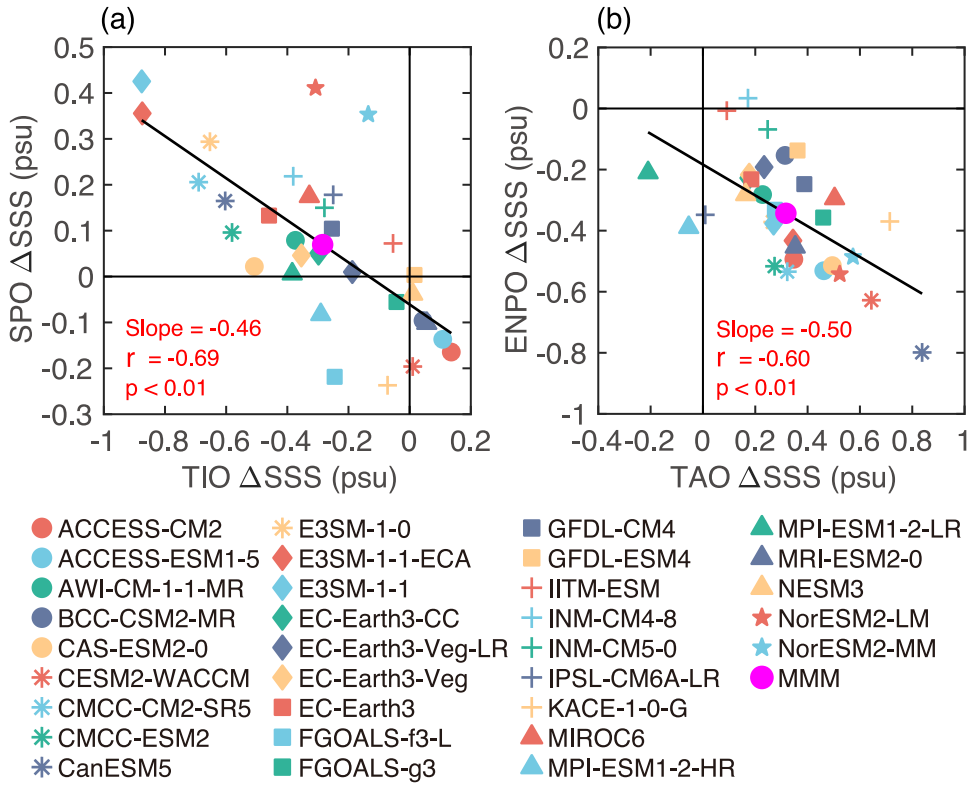

Figure 3. Correlations of projected SSS changes between paired regions. Scatter plots of annual-mean SSS changes (psu): (a) SPO versus TIO; (b) ENPO versus TAO. Each marker is one model. The black solid line shows the least-squares fit; slope, inter-model correlation (r), and p value are indicated on each panel. Anticorrelations highlight opposing basin responses central to the two-index framework.

bands toward the warmer hemisphere to restore the atmospheric energy balance (e.g., Friedman et al., 2013; Guilbert et al., 2024; Kaufmann & Stern, 1997; Stouffer et al., 1989), which energetically favors a northward displacement of tropical rainfall. Consistent with this, the SPO–TIO index is associated with intensified rainfall under the Pacific ITCZ and Indian summer monsoon regions (Bay of Bengal, eastern Arabian Sea), and reduced rainfall over the South Pacific Convergence Zone [SPCZ] (Figure 5b). Evaporation anomalies (Figure 5c) are modest (~0.1 mm day^{-1}) compared to precipitation changes (~0.5 mm day^{-1}), so inter-model E–P anomalies are predominantly rainfall-driven. Below, we analyze mechanisms separately for the TIO and SPO.

In CMIP6, inter-model differences in TIO E–P changes are dominated by precipitation ($r = -0.8$, $p < 0.01$; not shown), while evaporation plays little role ($r = 0.29$, $p = 0.1$; not shown). Precipitation strongly controls TIO SSS diversity ($r = -0.69$, $p < 0.01$; Figure 6a), with increased rainfall over the northern Indian Ocean (Figure 5b) driving the freshening. This robust correlation indicates that basin-scale TIO SSS changes are largely rainfall-driven, with evaporation and oceanic processes such as advection and mixing playing secondary roles. The freshening extends south of the rainfall maximum, suggesting that lateral advection by southward mean surface currents (green arrows in Figure 5a showing the MMM present-day circulation) likely redistributes freshwater within the basin. The rainfall increase itself scales with the tropical interhemispheric RSST gradient ($r = -0.62$, $p < 0.01$; Figure 6b), as relative Northern Hemisphere warming favors enhanced precipitation, consistent with previous studies (e.g., Bollasina et al., 2011; Friedman et al., 2013; Kang, 2020).

SPO SSS changes are also strongly linked to local precipitation ($r = -0.63$, $p < 0.01$; Figure 6c), with saltening reduced when rainfall increases. Evaporation plays little role ($r = 0.12$, $p = 0.5$; not shown). As in the TIO, SPO precipitation changes scale with the tropical interhemispheric RSST gradient ($r = 0.61$, $p < 0.01$; Figure 6d), and southward mean surface currents export salinity anomalies away from the SPCZ drying core, spreading saltening across the broader SPO (Figures 5a and 5b).

Table 2
Present-Day Salinity Contrasts and Projected Contrast Changes [ΔSSS] Between Basins in CMIP6

Inter-basin contrasts	MMM (psu)	MIN (psu)	MAX (psu)	STD (psu)
SPO–TIO ΔSSS	0.35	−0.3	1.3	0.42
TAO–ENPO ΔSSS	0.66	0	1.64	0.36
SPO–TIO present-day SSS	0.29	–	–	–
TAO–ENPO present-day SSS	1.05	–	–	–

Note. MMM denotes the multi-model mean, MIN the minimum, MAX the maximum, and STD the standard deviation across models. SPO–TIO denotes the SSS contrast between the southern Pacific (SPO) and the tropical Indian Ocean (TIO), while TAO–ENPO denotes that between the tropical Atlantic (TAO) and the equatorial-northern Pacific (ENPO).

The CMIP6 MMM projects a stronger SSS contrast between a fresher TIO and a saltier SPO in 2071–2100 relative to the present-day climatology (1985–2014). We have shown that inter-model diversity in this contrast correlates with interhemispheric RSST-gradient control of rainfall (ITCZ/monsoon intensification vs. SPCZ weakening), whereas evaporation changes contribute only weakly to the freshwater budget. Southward ocean currents then spread the resulting SSS anomalies, driving basin-wide freshening in the TIO and saltening across the SPO. This RSST-gradient linkage to the SPO–TIO index is strong ($r = -0.71$, $p < 0.01$; not shown), underscoring a common energetic driver of Indo-Pacific SSS diversity.

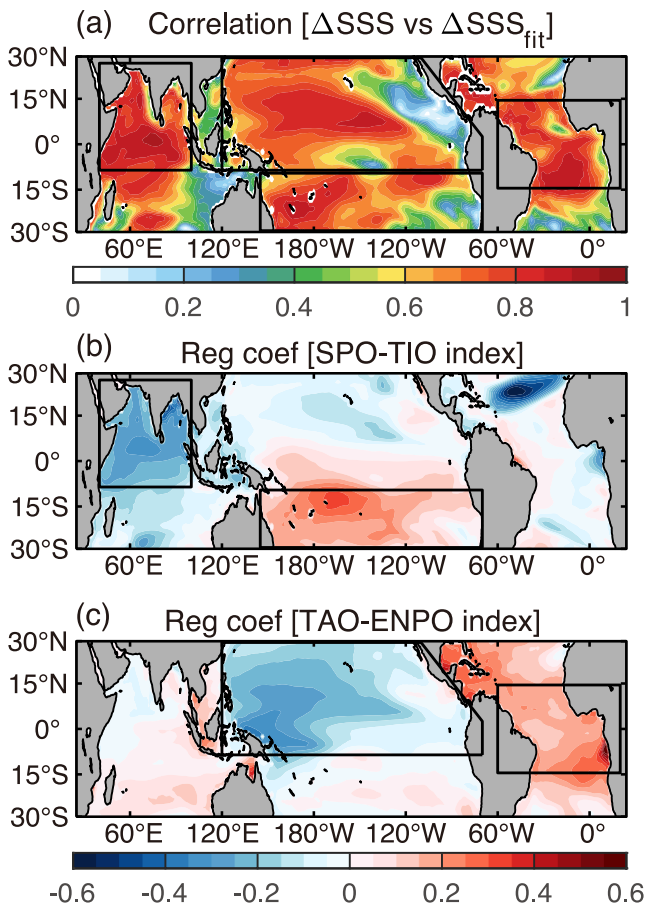

Figure 4. SSS patterns linked to two indices of inter-basin contrasts. (a) Correlation map between projected SSS changes and the multiple-linear-regression fit using the SPO–TIO ($I_{SPO-TIO}$) and TAO–ENPO ($I_{TAO-ENPO}$) indices. (b, c) Regression coefficient maps for (b) $I_{SPO-TIO}$ and (c) $I_{TAO-ENPO}$; coefficients represent the ΔSSS response per 1σ increase of the corresponding index, enabling direct comparison of amplitude. Black frames mark the TIO/SPO boxes in (b) and ENPO/TAO in (c). Correlations shown in (a) exceed ~0.7 over much of the tropics, indicating strong reconstruction skill.

5. Equatorial-Northern Pacific Ocean and Tropical Atlantic Ocean SSS Gradient Diversity

The CMIP6 MMM projects a stronger TAO–ENPO contrast, with a saltier tropical Atlantic and a fresher equatorial-northern Pacific. Below we examine the diversity in this projected contrast and its drivers. Figure 7 shows the SSS, rainfall, evaporation, and RSST changes regressed on the normalized TAO–ENPO index. In the Pacific, evaporation anomalies are small (below 0.15 mm day^{-1}) compared to rainfall changes that exceed 1 mm day^{-1} along the equator (Figures 7b and 7c). Over the Atlantic, rainfall changes are weaker and of mixed sign, while evaporation consistently increases, therefore playing a potential role in the freshwater budget (Figures 7b and 7c). Most rainfall anomalies occur in near-equatorial Pacific regions and coincide with enhanced equatorial warming (Figures 7b–7d), a pattern described in previous studies as "El Niño–like" (Xie et al., 2010). In the following, we analyze the mechanisms driving SSS diversity in the ENPO and TAO.

The intensity of ENPO freshening is strongly correlated with rainfall in the region across models ($r = -0.79$, $p < 0.01$; Figure 8a). This indicates a minor role for oceanic processes (advection, mixing) and a weak contribution of evaporation, as E–P changes are almost entirely controlled by precipitation ($r = -0.95$, $p < 0.01$; not shown), but they unexpectedly exhibit a negative correlation with evaporation ($r = -0.55$; not shown). Large equatorial Pacific rainfall anomalies account for about two-thirds of total ENPO rainfall changes (not shown). Previous studies have shown that a stronger "El Niño–like" RSST pattern enhances equatorial rainfall by destabilizing the atmosphere (Clement et al., 2010; Meehl et al., 2007; Xie et al., 2010). Consistently, ENPO rainfall is highly correlated with equatorial Pacific RSST changes ($r = 0.84$, $p < 0.01$; Figure 8b). Poleward surface currents in the northern Pacific likely spread the equatorial freshwater anomalies into the subtropics, extending the ENPO freshening (Figure 7a).

In contrast to the SPO, TIO and ENPO regions, TAO SSS changes are driven by evaporation ($r = 0.6$, $p < 0.01$; Figure 8c) rather than precipitation

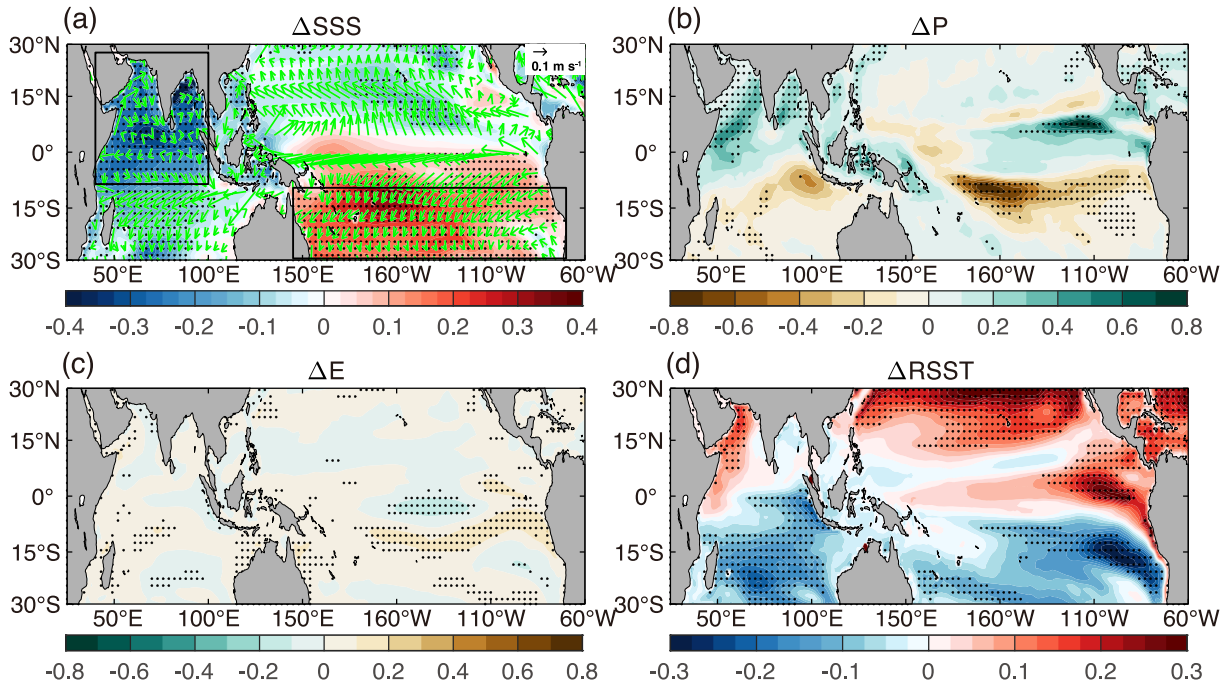

Figure 5. Projected changes associated with the SPO–TIO SSS contrast. Inter-model regressions of the annual-mean (a) SSS (psu), (b) precipitation $\left(\text{mm day}^{-1}\right)$, (c) evaporation $\left(\text{mm day}^{-1}\right)$, and (d) RSST (°C) changes onto $I_{SPO-TIO}$. Dots indicate regression coefficients that are different from zero at the 95% confidence level. Green arrows show MMM present-day near-surface oceanic currents, indicating pathways that redistribute freshwater anomalies. Black boxes denote TIO and SPO regions used in Figure 6.

($r = 0.08$, $p = 0.67$; not shown). The TAO is one of the few regions where evaporation dominates the inter-model spread of E–P changes ($r = 0.59$, $p < 0.01$; not shown). According to the Clausius–Clapeyron relation, evaporation should rise by 7% K^{-1} in the absence of wind or humidity changes (Allan et al., 2020; Zaitchik et al., 2023), a scaling that we indeed find across the tropics (not shown). In the TAO, however, the increase is weaker (4.2% K^{-1}; Figure 8d), likely because circulation changes (e.g., surface winds) partly offset the thermodynamic effect. Overall, models with stronger warming produce larger evaporation increases, leading to higher TAO SSS as evaporation outweighs precipitation in this region.

The CMIP6 MMM projects a stronger SSS contrast between a fresher ENPO and a saltier TAO. Inter-model diversity reflects two distinct mechanisms— rainfall-driven freshening in ENPO (linked to equatorial "El Niño–like" RSST) and thermodynamic evaporation-controlled saltening in TAO. The equatorial Pacific precipitation increase scales with the enhanced equatorial "El Niño–like" warming due to the "warmer gets wetter" mechanism, and the resulting equatorial freshening expands northward due to poleward surface mean currents. In the TAO, models that produce the largest warming also yield the largest evaporation and SSS increase through the thermodynamical "dry gets drier" mechanism.

6. Summary and Discussion

Previous studies have documented an increasing salinity contrast between tropical basins in both observations (Durack et al., 2012) and CMIP historical simulations (Terray et al., 2012). Consistent with earlier work based on earlier or smaller CMIP subsets (Capotondi et al., 2012; Li et al., 2023; Sathyanarayanan et al., 2021; Sun & Du, 2023), the CMIP6 MMM under SSP5-8.5 shows fresher TIO and ENPO and saltier SPO and TAO, but with substantial inter-model spread that has received less attention. Here we addressed this gap by organizing diversity with two independent inter-basin indices that together explain ~76% of the variance and by linking each index to distinct physical controls. The first reflects opposing changes between the TIO and SPO ($r \approx -0.7$), while the second captures opposite changes between the ENPO and TAO ($r \approx -0.6$). A schematic in Figure 9 summarizes the mechanisms associated with these two indices.

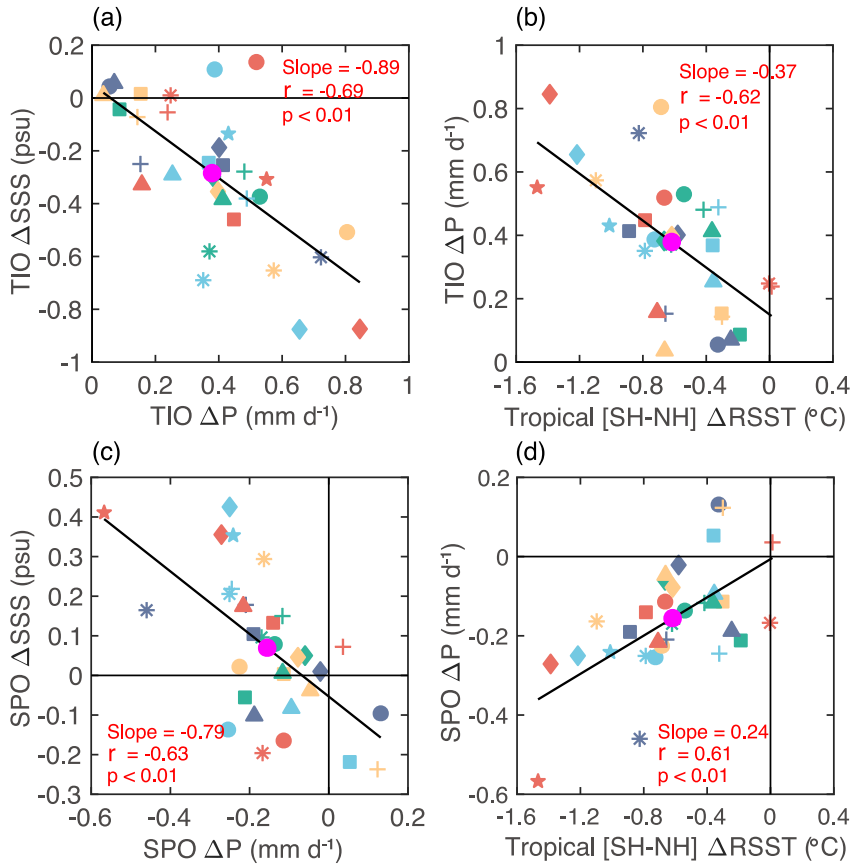

Figure 6. Mechanisms underlying inter-model spread in TIO and SPO. Scatter plots of annual-mean (a) TIO SSS change [ΔSSS] (psu) versus precipitation change [ΔP] $\left(\text{mm day}^{-1}\right)$, (b) TIO precipitation change $\left(\text{mm day}^{-1}\right)$ versus tropcial interhemispheric RSST-gradient change (°C), and the same for SPO in (c, d). Each marker is one model. Black solid lines show least-squares fits; slope, *r* and *p* values are given. Strong negative ΔSSS–ΔP correlations indicate rainfall-dominated freshwater control; gradient links in (b, d) emphasize energetic control of ITCZ/SPCZ shifts. Refer to Figure 3 for correspondence between CMIP6 models and symbols.

Diversity in the SPO–TIO contrast is tied to interhemispheric RSST-gradient changes (Figure 9a): relative Northern-Hemisphere warming favors ITCZ/monsoon strengthening over the northern Indian Ocean and drying over the SPCZ, with mean currents redistributing SSS anomalies basin-wide (freshening exported southward in TIO; saltening spread across SPO). The strong anticorrelation between SPO and TIO SSS changes arises because rainfall in both basins is tightly controlled by tropical-wide interhemispheric RSST gradients ($r = 0.84$ for Indian Ocean and $r = 0.95$ for Pacific Ocean, $p < 0.01$; Figures 10a and 10b).

For the TAO–ENPO contrast, two pathways share a common driver—the amplitude of tropical-mean warming (Figure 9b): in the Pacific, equatorial "El Niño–like" RSST increases bolster local rainfall, producing freshening that is exported poleward across the ENPO by mean currents, whereas in the Atlantic evaporation dominates and scales at ~4.2% K^{-1} (weaker than the ideal 7% K^{-1}), yielding saltening in TAO. Local TAO warming is tightly correlated with the tropical mean ($r = 0.98$, $p < 0.01$; Figure 10d), and equatorial Pacific warming also scales with it ($r = 0.69$, $p < 0.01$; Figure 10c). This scaling may reflect either the influence of Pacific warming patterns on clouds and the top-of-atmosphere radiation balance, thereby affecting climate sensitivity (Andrews et al., 2022), or the general tendency for regional warming contrasts to grow with global warming. Thus, the amplitude of tropical-mean warming emerges as a common driver of ENPO and TAO SSS changes acting through different pathways (rainfall in the Pacific, evaporation in the Atlantic).

Overall, our study confirms that tropical SSS is a useful "natural rain gauge" for tracking changes in the hydrological cycle (Cravatte et al., 2009; Curry et al., 2003; Durack et al., 2012; Durack & Wijffels, 2010; Helm et al., 2010; Hosoda et al., 2009; Schmitt, 2008; Skliris et al., 2014; Terray et al., 2012; Yu, 2011). Basin-scale

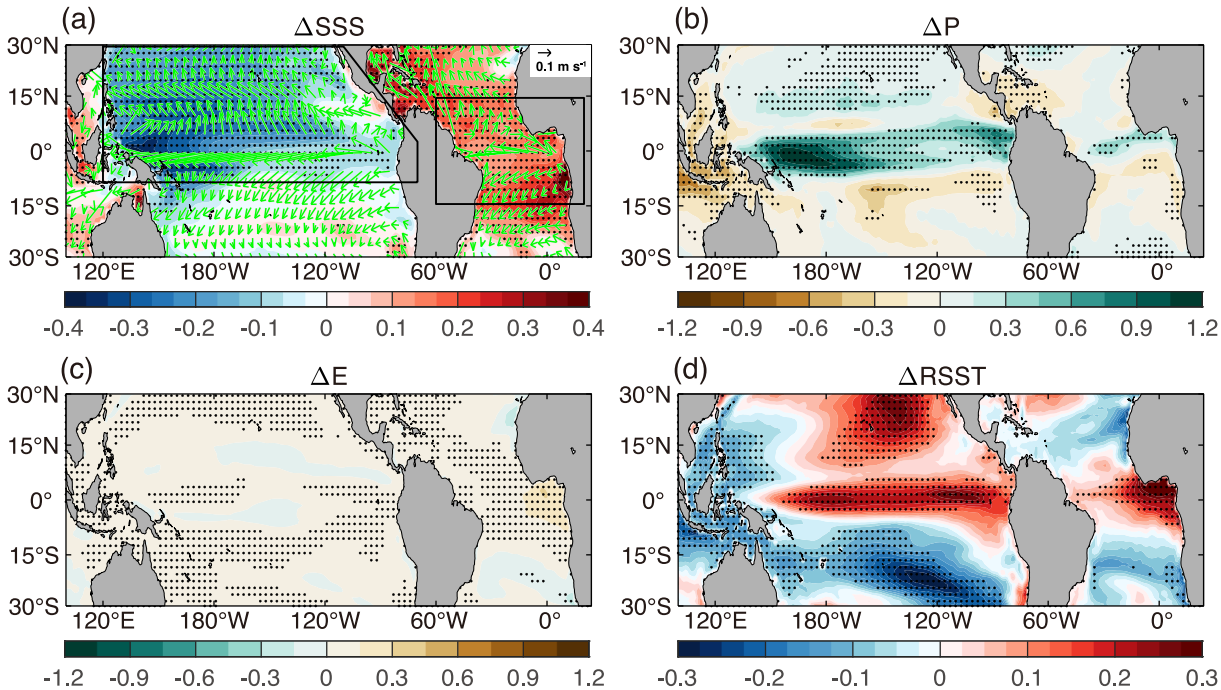

Figure 7. Projected changes associated with the TAO–ENPO SSS contrast. Inter-model regressions of the annual-mean (a) SSS (psu), (b) precipitation $\left(\text{mm day}^{-1}\right)$, (c) evaporation $\left(\text{mm day}^{-1}\right)$, and (d) RSST (°C) changes onto $I_{TAO-ENPO}$. Dots indicate regression coefficients that are different from zero at the 95% confidence level. Dots indicate regression coefficients that are different from zero at the 95% confidence level. Green arrows show MMM present-day near-surface oceanic currents, indicating pathways that redistribute freshwater anomalies. Black boxes denote ENPO and TAO regions used in Figure 8.

SSS changes indeed generally mirror E–P, consistent with Sathyanarayanan et al. (2021) and Sun and Du (2023), but advection by the mean circulation also plays a role by redistributing anomalies from localized freshwater sources or sinks across entire basins, consistent with Vinogradova and Ponte (2013) and Yu (2011).

We now turn to the limits of interpreting stronger SSS gradients solely as evidence of hydrological cycle intensification. Pattern correlations (Figure 11d) show that E–P changes—especially rainfall—align well with SSS changes ($r \approx 0.6$), consistent with a "wetter gets fresher" response (ΔE–P vs. ΔSSS) at large scales. Present-day SSS is also correlated with its projected change ($r \approx 0.7$), indicating that salty (fresh) regions tend to become saltier (fresher) –the classical "fresh gets fresher" pattern (present-day SSS vs. ΔSSS). This signal is especially pronounced for the Atlantic–Pacific contrast ($r \approx 0.75$; Figure 11c). However, enhanced "fresh gets fresher" gradients alone do not necessarily imply thermodynamic intensification. In CMIP6, rainfall and E–P changes bear little resemblance to the present-day rainfall distribution ($r < 0.2$; Figure 11a), and instead correlate more strongly with the warming pattern ($r \approx 0.55$; Figure 11b), consistent with the "warmer gets wetter" mechanism (ΔRSST vs. ΔE–P) highlighted in previous studies (Allan et al., 2020; Zaitchik et al., 2023).

The Atlantic stands out as the only tropical basin where thermodynamics dominate: evaporation is the primary driver of SSS change, and the magnitude of warming controls the strength of both enhanced evaporation and the resulting saltening. By contrast, projected Indo-Pacific changes are governed mainly by rainfall anomalies that are ultimately anchored to SST patterns ("warmer gets wetter"). Consequently, the resemblance between the future "fresh gets fresher" pattern and today's salinity climatology is only partly causal; it largely reflects a warming pattern that intensifies rainfall over the already fresh equatorial-northern Pacific, deepening its contrast with the Atlantic. We therefore view detectable SSS trends as fingerprints of hydrological-cycle change, while emphasizing that they reflect not only thermodynamic intensification but also substantial SST-pattern–driven circulation and rainfall shifts.

Our inferences are statistical and intended to guide process-based testing. In reality, SSS changes reflect both surface freshwater fluxes and circulation-driven processes. The lack of spatial collocation between E–P and SSS changes in several regions (e.g., tropical Pacific and Indian Oceans; Figures 5 and 7) indicates a substantial role

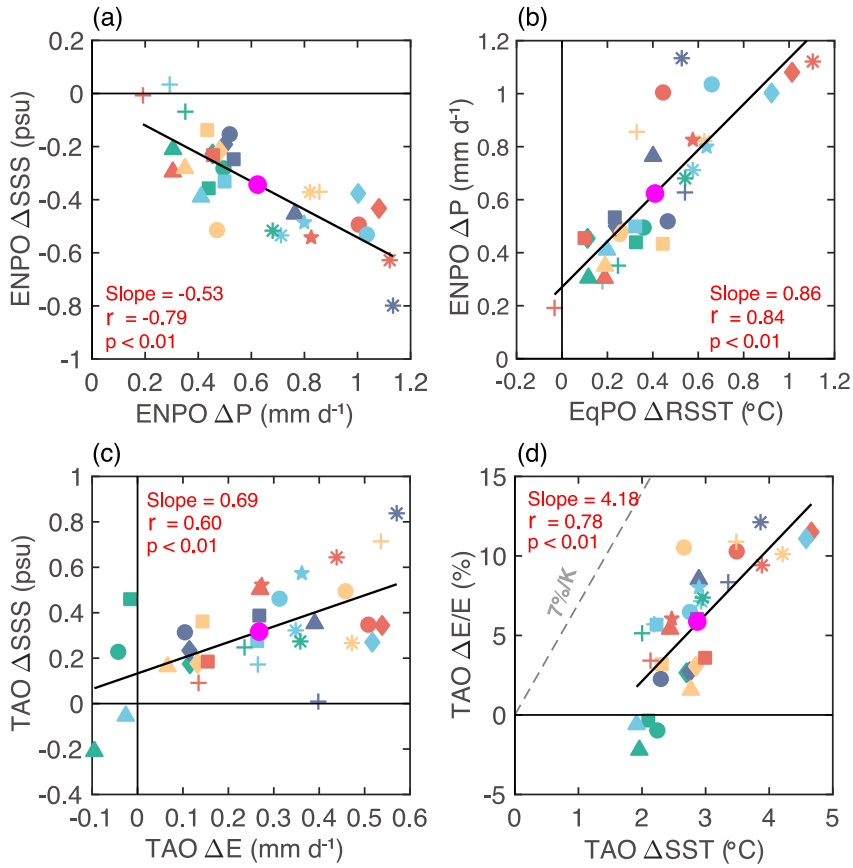

Figure 8. Mechanisms underlying inter-model spread in ENPO and TAO. Scatter plots for ENPO: (a) SSS change (psu) versus precipitation change $\left(\text{mm day}^{-1}\right)$, (b) precipitation change $\left(\text{mm day}^{-1}\right)$ versus equatorial-Pacific mean RSST change (°C); for TAO: (c) SSS change (psu) versus evaporation change $\left(\text{mm day}^{-1}\right)$, (d) (evaporation change/present-day evaporation) (%) versus local SST change (°C). Each marker is one model. Black solid lines show least-squares fits; slope, *r* and *p* values are given. Panels (b, d) diagnose, respectively, "warmer gets wetter" RSST control in the Pacific and sub-Clausius–Clapeyron (~4.2% K^{-1}) evaporation scaling in the Atlantic. Refer to Figure 3 for correspondence between CMIP6 models and symbols.

for ocean dynamics in shaping the SSS changes. Changes in wind stress modify advection, upwelling, and mixing, all of which influence SSS. Targeted ocean model experiments forced with projected surface-flux changes are needed to quantify the relative roles of E–P versus circulation in shaping regional SSS responses. Complementary atmospheric GCM experiments can separate sensitivity to warming patterns from mean tropical warming.

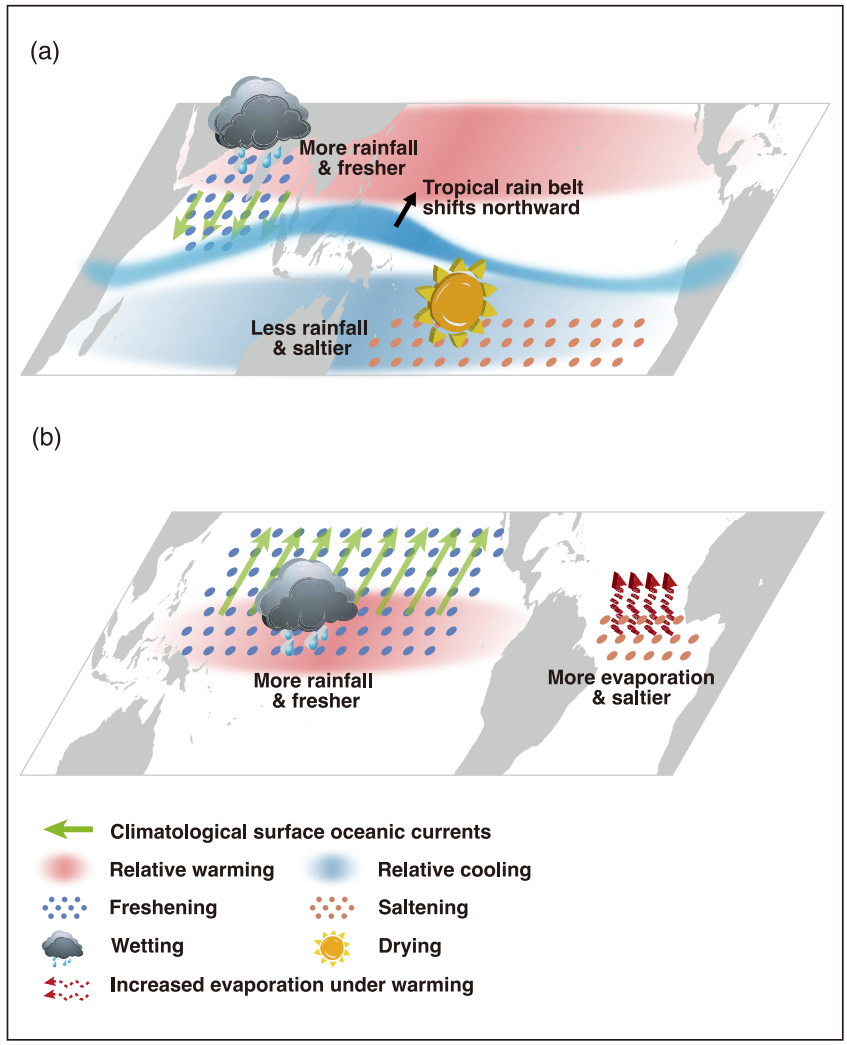

Figure 9. Controls on inter-model diversity of tropical SSS changes (schematic). (a) Interhemispheric RSST-gradient control (relative Northern-Hemisphere warming/Sorthern-Hemisphere cooling) shifts the rain belt northward, enhancing monsoon/ITCZ rainfall (freshening) and weakening SPCZ rainfall (saltening); green arrows depict climatological surface currents that spread anomalies. (b) Tropical-mean warming control: equatorial Pacific "El Niño–like" RSST increases intensify rainfall (ENPO freshening), while enhanced evaporation under warming raises TAO salinity. Red/blue shading denotes relative warming/cooling; clouds/blue stipples indicate wetting/freshening; suns/orange stipples indicate drying/saltening.

10.1029/2025EF007346

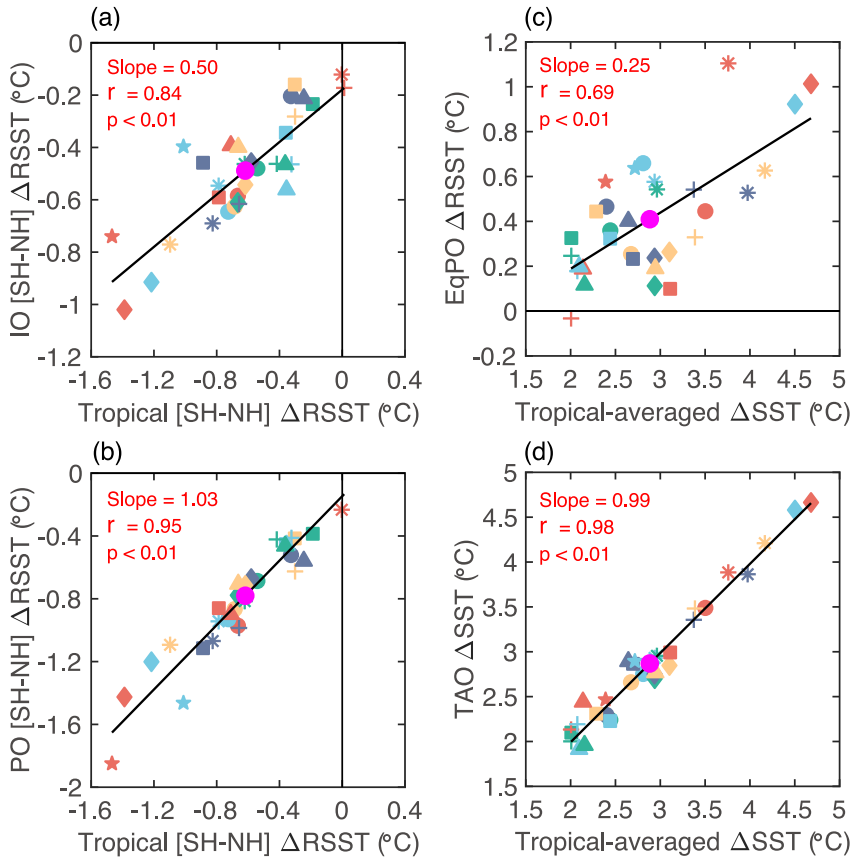

Figure 10. Linkage with interhemispheric RSST gradient and tropical warming. Scatter plots of tropical interhemispheric RSST-gradient change versus basin interhemispheric RSST-gradient change for the (a) Indian Ocean and (b) Pacific Ocean; (c) tropical-mean warming (°C) versus equatorial-Pacific RSST change (°C); (d) tropical-mean warming (°C) versus TAO SST change (°C). Each marker is one model. Black solid lines show least-squares fits; slope, r and p values are given. Local TAO warming scales tightly with the tropical mean ($r = 0.98$; panel d), while equatorial-Pacific warming also scales with it ($r = 0.69$; panel c), highlighting a common driver for the TAO–ENPO contrast. Refer to Figure 3 for correspondence between CMIP6 models and symbols.

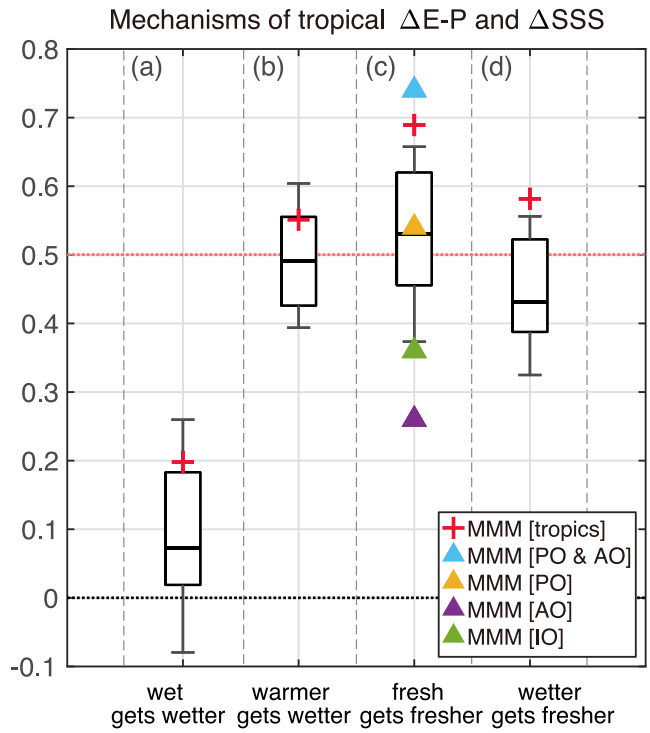

Figure 11. Testing tropical SSS and E–P changes mechanisms. Each box plot represents the CMIP6 inter-model distribution of tropical (within 30°S–30°N) pattern correlation between various quantities: (a) present-day freshwater flux and its change (E–P vs. ΔE–P) for "wet gets wetter," (b) RSST change and precipitation change (ΔRSST vs. ΔP) for "warmer gets wetter," (c) present-day SSS and its change (SSS vs. ΔSSS) for "fresh gets fresher," (d) freshwater flux change and SSS change (ΔE–P vs. ΔSSS) for "wetter gets fresher." The central horizontal line of each box indicates the median, the box edges the 25th and 75th percentiles and the whiskers the 10th and 90th percentiles. The red crosses indicate pattern correlations for the CMIP6 MMM. In panel (c), the colored triangles correspond to correlations computed over the full tropical Pacific (yellow), Atlantic (purple), Indian (green), and Pacific–Atlantic (blue) basins (30°S–30°N). These basin domains differ from the smaller regional boxes used earlier. We include triangles only in panel (c) because this panel evaluates basin-scale "fresh gets fresher" relationships. This representation clarifies that the dominant signal arises primarily from the Pacific–Atlantic contrast. Panels (b–d) underscore that rainfall anomalies align more with RSST patterns (than with present-day rainfall), that present-day SSS relates to its change ($r \approx 0.7$), and that ΔSSS tracks freshwater forcing ($r \approx 0.6$).

Conflict of Interest

The authors declare no conflicts of interest relevant to this study.

Data Availability Statement

This study is based on CMIP6 output. They are publicly available online at https://aims2.llnl.gov/search/cmip6/. Users should select the models and variables as indicated in Table 1, the variant label as r1i1p1f1, the frequency as monthly, and the experiment ID as historical and ssp585. The software and analysis scripts used to generate the results and figures can be accessed using the following DOI link: https://doi.org/10.5281/zenodo.17704585 (Pang, 2025).

Acknowledgments

We acknowledge the Program for Climate Model Diagnosis and Intercomparison and the World Climate Research Programme (WCRP) Working Group on Coupled Modeling for their roles in making the WCRP CMIP6 multi-model data set available. We appreciate insightful suggestions from Dr. Juliette Mignot regarding the Atlantic Ocean. This study benefited from the IPSL Data and Computing Center ESPRI which is supported by CNRS, SU, CNES and Ecole Polytechnique. S. Pang gratefully acknowledges Sorbonne University and the LOCEAN laboratory for providing a quality working environment. The authors thank the editor and the three anonymous reviewers for their valuable comments.

References

Akhil, V. P., Lengaigne, M., Durand, F., Vialard, J., Chaitanya, A. V. S., Keerthi, M. G., et al. (2016). Assessment of seasonal and year-to-year surface salinity signals retrieved from SMOS and Aquarius missions in the Bay of Bengal. *International Journal of Remote Sensing*, *37*(5), 1089–1114. https://doi.org/10.1080/01431161.2016.1145362

Allan, R. P., Barlow, M., Byrne, M. P., Cherchi, A., Douville, H., Fowler, H. J., et al. (2020). Advances in understanding large-scale responses of the water cycle to climate change. *Annals of the New York Academy of Sciences*, *1472*(1), 49–75. https://doi.org/10.1111/nyas.14337

Allen, M. R., & Ingram, W. J. (2002). Constraints on future changes in climate and the hydrologic cycle. *Nature*, *419*(6903), 224–232. https://doi.org/10.1038/nature01092

Andrews, T., Bodas-Salcedo, A., Gregory, J. M., Dong, Y., Armour, K. C., Paynter, D., et al. (2022). On the effect of historical SST patterns on radiative feedback. *Journal of Geophysical Research: Atmospheres*, *127*(18), e2022JD036675. https://doi.org/10.1029/2022jd036675

Balaguru, K., Foltz, G. R., Leung, L. R., Kaplan, J., Xu, W., Reul, N., & Chapron, B. (2020). Pronounced impact of salinity on rapidly intensifying tropical cyclones. *Bulletin of the American Meteorological Society*, *101*(9), E1497–E1511. https://doi.org/10.1175/bams-d-19-0303.1

Bollasina, M. A., Ming, Y., & Ramaswamy, V. (2011). Anthropogenic aerosols and the weakening of the South Asian summer monsoon. *Science*, *334*(6055), 502–505. https://doi.org/10.1126/science.1204994

Capotondi, A., Alexander, M. A., Bond, N. A., Curchitser, E. N., & Scott, J. D. (2012). Enhanced upper ocean stratification with climate change in the CMIP3 models. *Journal of Geophysical Research*, *117*(C4). https://doi.org/10.1029/2011jc007409

Chou, C., & Neelin, J. D. (2004). Mechanisms of global warming impacts on regional tropical precipitation. *Journal of Climate*, *17*(13), 2688–2701. https://doi.org/10.1175/1520-0442(2004)017<2688:mogwio>2.0.co;2

Chung, C. E., & Ramanathan, V. (2006). Weakening of North Indian SST gradients and the monsoon rainfall in India and the Sahel. *Journal of Climate*, *19*(10), 2036–2045. https://doi.org/10.1175/jcli3820.1

Clement, A. C., Baker, A. C., & Leloup, J. (2010). Patterns of tropical warming. *Nature Geoscience*, *3*(1), 8–9. https://doi.org/10.1038/ngeo728

Cravatte, S., Delcroix, T., Zhang, D., McPhaden, M., & Leloup, J. (2009). Observed freshening and warming of the western Pacific warm pool. *Climate Dynamics*, *33*(4), 565–589. https://doi.org/10.1007/s00382-009-0526-7

Curry, R., Dickson, B., & Yashayaev, I. (2003). A change in the freshwater balance of the Atlantic Ocean over the past four decades. *Nature*, *426*(6968), 826–829. https://doi.org/10.1038/nature02206

Du, Y., Zhang, Y., Feng, M., Wang, T., Zhang, N., & Wijffels, S. (2015). Decadal trends of the upper ocean salinity in the tropical Indo-Pacific since mid-1990s. *Scientific Reports*, *5*(1), 16050. https://doi.org/10.1038/srep16050

Durack, P. J., & Wijffels, S. E. (2010). Fifty-year trends in global ocean salinities and their relationship to broad-scale warming. *Journal of Climate*, *23*(16), 4342–4362. https://doi.org/10.1175/2010jcli3377.1

Durack, P. J., Wijffels, S. E., & Matear, R. J. (2012). Ocean salinities reveal strong global water cycle intensification during 1950 to 2000. *Science*, *336*(6080), 455–458. https://doi.org/10.1126/science.1212222

Eyring, V., Bony, S., Meehl, G. A., Senior, C. A., Stevens, B., Stouffer, R. J., & Taylor, K. E. (2016). Overview of the coupled model intercomparison project phase 6 (CMIP6) experimental design and organization. *Geoscientific Model Development*, *9*(5), 1937–1958. https://doi.org/10.5194/gmd-9-1937-2016

Friedman, A. R., Hwang, Y.-T., Chiang, J. C., & Frierson, D. M. (2013). Interhemispheric temperature asymmetry over the twentieth century and in future projections. *Journal of Climate*, *26*(15), 5419–5433. https://doi.org/10.1175/jcli-d-12-00525.1

Ge, K., Li, Y., Lyu, Y., Lin, P., Cheng, L., & Wang, F. (2023). Surface salinity changes of the tropical and subtropical oceans since 1970 and their relationship with surface freshwater fluxes. *Journal of Geophysical Research: Oceans*, *128*(12), e2023JC020207. https://doi.org/10.1029/2023jc020207

Guilbert, M., Terray, P., Mignot, J., Ollier, L., & Gastineau, G. (2024). Interhemispheric temperature gradient and equatorial Pacific SSTs drive Sahel monsoon uncertainties under global warming. *Journal of Climate*, *37*(3), 1033–1052. https://doi.org/10.1175/jcli-d-23-0162.1

He, F., & Clark, P. U. (2022). Freshwater forcing of the Atlantic meridional overturning circulation revisited. *Nature Climate Change*, *12*(5), 449–454. https://doi.org/10.1038/s41558-022-01328-2

Held, I. M., & Soden, B. J. (2006). Robust responses of the hydrological cycle to global warming. *Journal of Climate*, *19*(21), 5686–5699. https://doi.org/10.1175/jcli3990.1

Helm, K. P., Bindoff, N. L., & Church, J. A. (2010). Changes in the global hydrological-cycle inferred from ocean salinity. *Geophysical Research Letters*, *37*(18). https://doi.org/10.1029/2010gl044222

Hochet, A., Tajouri, S., Kolodziejczyk, N., & Llovel, W. (2025). Mechanisms of tropical sea surface salinity variations at seasonal timescales. *Journal of Geophysical Research: Oceans*, *130*(2), e2024JC021455. https://doi.org/10.1029/2024jc021455

Hosoda, S., Suga, T., Shikama, N., & Mizuno, K. (2009). Global surface layer salinity change detected by Argo and its implication for hydrological cycle intensification. *Journal of Oceanography*, *65*(4), 579–586. https://doi.org/10.1007/s10872-009-0049-1

Huntington, T. G. (2006). Evidence for intensification of the global water cycle: Review and synthesis. *Journal of Hydrology*, *319*(1–4), 83–95. https://doi.org/10.1016/j.jhydrol.2005.07.003

IPCC. (2021). In. *Climate change 2021: The physical science basis. Contribution of working group I to the sixth assessment report of the intergovernmental panel on climate change* Eds. V. Masson-Delmotte et al. [Book]. Cambridge University Press. https://doi.org/10.1017/9781009157896

Izumo, T., Vialard, J., Lengaigne, M., & Suresh, I. (2020). Relevance of relative sea surface temperature for tropical rainfall interannual variability. *Geophysical Research Letters*, *47*(3), e2019GL086182. https://doi.org/10.1029/2019gl086182

Kang, S. M. (2020). Extratropical influence on the tropical rainfall distribution. *Current Climate Change Reports*, *6*(1), 24–36. https://doi.org/10.1007/s40641-020-00154-y

Kaufmann, R. K., & Stern, D. I. (1997). Evidence for human influence on climate from hemispheric temperature relations. *Nature*, *388*(6637), 39–44. https://doi.org/10.1038/40332

Khosravi, N., Wang, Q., Koldunov, N., Hinrichs, C., Semmler, T., Danilov, S., & Jung, T. (2022). The Arctic Ocean in CMIP6 models: Biases and projected changes in temperature and salinity. *Earth's Future*, *10*(2), e2021EF002282. https://doi.org/10.1029/2021ef002282

Li, G., Cheng, L., & Wang, X. (2023). Evaluation of the CAS-ESM2-0 performance in simulating the global ocean salinity change. *Atmosphere*, *14*(1), 107. https://doi.org/10.3390/atmos14010107

Liu, Y., & Chiang, J. (2012). Coordinated abrupt weakening of the Eurasian and North African monsoons in the 1960s and links to extratropical North Atlantic cooling. *Journal of Climate*, *25*(10), 3532–3548. https://doi.org/10.1175/jcli-d-11-00219.1

Manabe, S., & Stouffer, R. J. (1995). Simulation of abrupt climate change induced by freshwater input to the North Atlantic Ocean. *Nature*, *378*(6553), 165–167. https://doi.org/10.1038/378165a0

Meehl, G. A., Stocker, T. F., Collins, W. D., Friedlingstein, P., Gaye, A. T., Gregory, J. M., et al. (2007). Global climate projections. In *Climate change 2007: The physical science basis. Contribution of working group I to the fourth assessment report of the intergovernmental panel on climate change*. Cambridge University Press.

Pang, S. (2025). Earth's future "Tropical Salinity Contrast Strengthening in CMIP6: Inter-model Diversity and Mechanisms" – Software (version v2) [Software]. *Zenodo*. https://doi.org/10.5281/zenodo.17704585

Rahmstorf, S. (1995). Bifurcations of the Atlantic thermohaline circulation in response to changes in the hydrological cycle. *Nature*, *378*(6553), 145–149. https://doi.org/10.1038/378145a0

Roderick, M. L., Greve, P., & Farquhar, G. D. (2015). On the assessment of aridity with changes in atmospheric CO_2. *Water Resources Research*, *51*(7), 5450–5463. https://doi.org/10.1002/2015wr017031

Sathyanarayanan, A., Köhl, A., & Stammer, D. (2021). Ocean salinity changes in the global ocean under global warming conditions. Part I: Mechanisms in a strong warming scenario. *Journal of Climate*, *34*(20), 8219–8236.

Schmitt, R. W. (2008). Salinity and the global water cycle. *Oceanography*, *21*(1), 12–19. https://doi.org/10.5670/oceanog.2008.63

Shu, Q., Qiao, F., Song, Z., Zhao, J., & Li, X. (2018). Projected freshening of the Arctic Ocean in the 21st century. *Journal of Geophysical Research: Oceans*, *123*(12), 9232–9244. https://doi.org/10.1029/2018jc014036

Skliris, N., Marsh, R., Josey, S. A., Good, S. A., Liu, C., & Allan, R. P. (2014). Salinity changes in the World Ocean since 1950 in relation to changing surface freshwater fluxes. *Climate Dynamics*, *43*(3–4), 709–736. https://doi.org/10.1007/s00382-014-2131-7

Stouffer, R., Manabe, S., & Bryan, K. (1989). Interhemispheric asymmetry in climate response to a gradual increase of atmospheric CO_2. *Nature*, *342*(6250), 660–662. https://doi.org/10.1038/342660a0

Sun, & Du, Y. (2023). Sea surface salinity changes and trans-basin water vapor transport between the Atlantic and Pacific under CMIP6 abrupt-4x CO_2 scenario. *Climate Dynamics*, *60*(5), 1907–1924. https://doi.org/10.1007/s00382-022-06385-z

Sun, Du, Y., Xie, S.-P., Zhang, Y., Wang, M., & Kosaka, Y. (2021). Sea surface salinity change since 1950: Internal variability versus anthropogenic forcing. *Journal of Climate*, *34*(4), 1305–1319. https://doi.org/10.1175/jcli-d-20-0331.1

Terray, L., Corre, L., Cravatte, S., Delcroix, T., Reverdin, G., & Ribes, A. (2012). Near-surface salinity as nature's rain gauge to detect human influence on the tropical water cycle. *Journal of Climate*, *25*(3), 958–977. https://doi.org/10.1175/jcli-d-10-05025.1

Thouvenin-Masson, C., Boutin, J., Échevin, V., Lazar, A., & Vergely, J.-L. (2024). Influence of river runoff and precipitation on the seasonal and interannual variability of sea surface salinity in the eastern North Tropical Atlantic. *Ocean Science*, *20*(6), 1547–1566. https://doi.org/10.5194/os-20-1547-2024

Van Oldenborgh, G. J., Hendon, H., Stockdale, T., L'Heureux, M., De Perez, E. C., Singh, R., & Van Aalst, M. (2021). Defining El Niño indices in a warming climate. *Environmental Research Letters*, *16*(4), 044003. https://doi.org/10.1088/1748-9326/abe9ed

Vialard, J., & Delecluse, P. (1998). An OGCM study for the TOGA decade. Part II: Barrier-layer formation and variability. *Journal of Physical Oceanography*, *28*(6), 1089–1106. https://doi.org/10.1175/1520-0485(1998)028<1089:aosftt>2.0.co;2

Vinogradova, N. T., & Ponte, R. M. (2013). Clarifying the link between surface salinity and freshwater fluxes on monthly to interannual time scales. *Journal of Geophysical Research: Oceans*, *118*(6), 3190–3201. https://doi.org/10.1002/jgrc.20200

Wang, H., Hu, S., Guan, C., & Li, X. (2024). The role of sea surface salinity in ENSO forecasting in the 21st century. *npj Climate and Atmospheric Science*, *7*(1), 206. https://doi.org/10.1038/s41612-024-00763-6

Williams, P. D., Guilyardi, E., Sutton, R., Gregory, J., & Madec, G. (2007). A new feedback on climate change from the hydrological cycle. *Geophysical Research Letters*, *34*(8). https://doi.org/10.1029/2007gl029275

Xie, S.-P., Deser, C., Vecchi, G. A., Ma, J., Teng, H., & Wittenberg, A. T. (2010). Global warming pattern formation: Sea surface temperature and rainfall. *Journal of Climate*, *23*(4), 966–986. https://doi.org/10.1175/2009jcli3329.1

Yu, L. (2011). A global relationship between the ocean water cycle and near-surface salinity. *Journal of Geophysical Research*, *116*(C10), C10025. https://doi.org/10.1029/2010jc006937

Zaitchik, B. F., Rodell, M., Biasutti, M., & Seneviratne, S. I. (2023). Wetting and drying trends under climate change. *Nature Water*, *1*(6), 502–513. https://doi.org/10.1038/s44221-023-00073-w

Zika, J. D., Skliris, N., Blaker, A. T., Marsh, R., Nurser, A. G., & Josey, S. A. (2018). Improved estimates of water cycle change from ocean salinity: The key role of ocean warming. *Environmental Research Letters*, *13*(7), 074036. https://doi.org/10.1088/1748-9326/aace42